PCCP

Cite this: *Phys. Chem. Chem. Phys.*, 2012, **14**, 675–680

www.rsc.org/pccp

PAPER

Photodissociation of isobutene at 193 nm

Gabriel M. P. Just,[ab] Bogdan Negru,[ab] Dayoung Park[ab] and Daniel M. Neumark*[ab]

Received 19th August 2011, Accepted 28th October 2011
DOI: 10.1039/c1cp22651g

The collisionless photodissociation dynamics of isobutene (*i*-C_4H_8) at 193 nm *via* photofragment translational spectroscopy are reported. Two major photodissociation channels were identified: H + C_4H_7 and CH_3 + CH_3CCH_2. Translational energy distributions indicate that both channels result from statistical decay on the ground state surface. Although the CH_3 loss channel lies 13 kcal mol^{-1} higher in energy, the CH_3 : H branching ratio was found to be 1.7 (5), in reasonable agreement with RRKM calculations.

I. Introduction

Isobutene, *i*-C_4H_8, (2-methylpropene) is the smallest branched alkene. It plays a key role in combustion chemistry as an intermediate in the pyrolysis of *iso*-octane and in the oxidation of fuel additives such as MTBE and ETBE (methyl and ethyl *t*-butyl ether).[1] The chemistry of isobutene in the Earth's troposphere, notably its reactions with NO_2 and NO_3,[2,3] is of interest, as are its reactions with free radicals in the atmosphere of Titan in order to form larger hydrocarbons.[4] Isobutene has been implicated as a product in the $O(^3P)$ + *t*-C_4H_9(*t*-butyl) radical–radical reaction[5] and from the photodissociation of *tert*-C_4H_9.[6,7] However, the photodissociation of isobutene itself has not been reported previously. In this paper, we investigate the collisionless photodissociation of isobutene at 193 nm in order to gain new insights into its unimolecular photochemistry and dissociation dynamics.

The work presented here is motivated by numerous studies of the bimolecular and unimolecular kinetics of isobutene in shock tubes and flames.[8–13] These studies have focused on elucidating the mechanisms for the oxidation and pyrolysis of isobutene. An issue arising from this body of work is the identity of the products arising from the unimolecular decay of isobutene. In some kinetics studies, reaction mechanisms are proposed in which only H atom loss is included,[10,12] whereas others also include the somewhat higher energy CH_3 loss channel.[8,13,14] Photodissociation measurements provide unambiguous identification of the primary products from photoexcitation to an excited electronic state. In cases where dissociation proceeds *via* internal conversion to the ground state followed by statistical decay, the results of photodissociation experiments can have direct bearing on the interpretation of kinetics experiments in which it is often very difficult to identify product channels for specific reactions.

Photodissociation of isobutene is also of interest in light of previous work by Zierhut *et al.*[6] and our group[7] on the photodissociation of the *t*-C_4H_9 radical near 248 nm. One concern in those experiments was that some observed channels were from the photodissociation of vibrationally hot isobutene produced in the pyrolysis source used to generate *t*-butyl radical rather than from *t*-butyl itself. An independent study of isobutene photodissociation could thus corroborate the interpretation of the previous experiments on *t*-butyl.

The UV absorption spectrum of the isobutene molecule begins around 205 nm and comprises numerous closely spaced bands;[15,16] the band around 193 nm has been assigned to the lowest-lying ππ* transition.[17,18] Excitation at 193 nm can lead to photodissociation by two bond cleavage channels involving loss of either an H atom or a CH_3 group:

$$(CH_3)_2CCH_2 + h\nu \rightarrow \cdot CH_2CH_3CCH_2 + H \quad \Delta H_0 = 88.3 \text{ kcal mol}^{-1},[19] \quad (1)$$

$$(CH_3)_2CCH_2 + h\nu \rightarrow CH_3C\cdot CH_2 + CH_3 \quad \Delta H_0 = 100.9 \text{ kcal mol}^{-1}, \quad (2)$$

The 2-methylallyl radical from channel 1, can further dissociate to form allene (C_3H_4) *via* the loss of a methyl group.[20] The barrier to this dissociation process has been calculated by Li *et al.*[21] to be 55.5 kcal mol^{-1}. Furthermore, the 2-propenyl radical from channel 2 can undergo a 1,2-hydrogen shift over an isomerization barrier of 45.4 kcal mol^{-1} to form the allyl radical.[22] Fig. 1 shows the primary energetics for channels 1 and 2 as well as the barrier heights and energies for subsequent dissociation and isomerization.

In this work, we investigate the collisionless photodissociation of isobutene at 193 nm using molecular beam photofragment translational spectroscopy. This experiment yields the kinetic energy and angular distribution for each photofragmentation channel, enabling the direct identification of the primary photofragments and providing insight into the dissociation mechanism.

[a] *Department of Chemistry, University of California, Berkeley, CA 94720, USA. E-mail: dneumark@berkeley.edu*
[b] *Chemical Sciences Division, Lawrence Berkeley National Laboratory, Berkeley, CA 94720, USA*

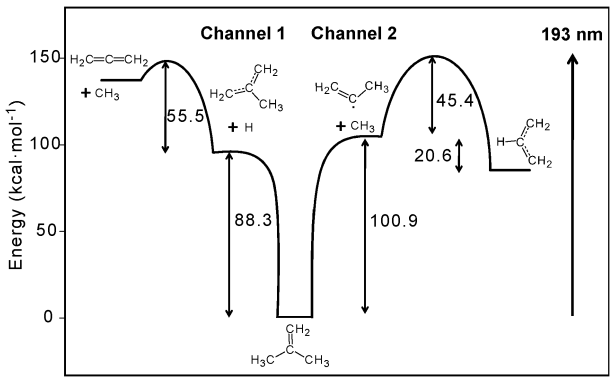

Fig. 1 Potential energy surface of isobutene based on ref. 21 and 22.

We find here that both channels 1 and 2 occur with kinetic energy distributions consistent with statistical decay on the ground state surface. The branching ratio is about 1.7 (5) in favor of the higher energy channel 2. These results are interpreted based on simple RRKM considerations.

II. Experimental

The molecular beam photodissociation apparatus has been described in previous papers[23–25] and is shown in Fig. 2. A fixed molecular beam is intersected by a pulsed laser and a rotatable detector is used to analyze the photodissociation products *via* electron impact ionization mass spectroscopy. Photofragment time-of-flight measurements for ion masses of interest are taken at a variety of laboratory scattering angles Θ_{lab}.

In more detail, a pulsed molecular beam of isobutene was formed using a piezo-activated valve (Physik Intrumente, PI) at a repetition rate of 200 Hz. The gas mixture was 1% isobutene (purity greater than 99%, SynQuest Labs Inc, FL) in helium or neon with a backing pressure of 25 psig. The molecular beam was collimated with two skimmers, one of which separated the source chamber from the main chamber where dissociation and detection occurs. In the main chamber, the molecular beam was crossed at a 90° by a focused photodissociation beam (2 × 4 mm) produced by an ArF (193 nm) excimer laser (Lambda-Physik) operating at a repetition rate of 100 Hz with a typical pulse energy of 40 mJ. The scattered photofragments were detected in the plane defined by the molecular and laser beams as a function of the laboratory angle, Θ_{lab}, measured with respect to the molecular beam. After reaching the triply differentially pumped detection region, the neutral photofragments were ionized by electron impact ionization (77 eV), mass-selected using a quadrupole mass spectrometer, and observed with a Daly style ion detector. Photofragment time of flight (TOF) spectra with respect to the laser pulse were obtained by measuring ion signal as a function of time and were digitally recorded by the use of a multichannel scaler connected to a PC-computer. Spectra in which helium was the carrier gas were accumulated over 50 000 laser shots; the data acquisition time was increased to 2-300 000 laser shots when Ne was used as the carrier gas. Background subtraction was performed in order to only observe signal relevant to the photodissociation of isobutene.

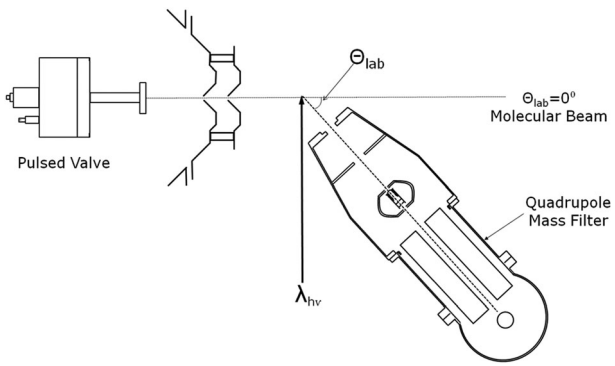

Fig. 2 Schematic representation of the apparatus, showing the molecular beam source, the photodissociation laser and the rotating mass spectrometer detector.

The molecular beam was characterized using a slotted chopper spinning at a 200 Hz. Characteristic beam velocities of about 1700 m s^{-1} were obtained in the present experiment using He as a seed gas. The corresponding speed ratio (beam flow velocity over velocity spread) was consistently in the range of 35–40. When using Ne as a carrier gas, typical beam velocities were 800 m s^{-1} with a speed ratio of 20.

III. Results

Fig. 3 shows representative TOF data at m/z = 55 ($C_4H_7^+$), the parent ion for the C_4H_7 fragment that would be formed by H atom loss *via* channel 1. Three of these spectra were taken using He as the seeding gas, while the fourth, at Θ = 9°, was taken with Ne as the carrier gas. Fig. 4 shows spectra at m/z = 41 ($C_3H_5^+$) and m/z = 15 (CH_3^+), corresponding to the parent ions for channel 2. These spectra were taken with He as the carrier gas. In all TOF spectra, open circles represent the data and the solid lines represent the simulated fit to the data obtained using forward convolution of assumed center-of-mass translational energy distributions (see Section IV).

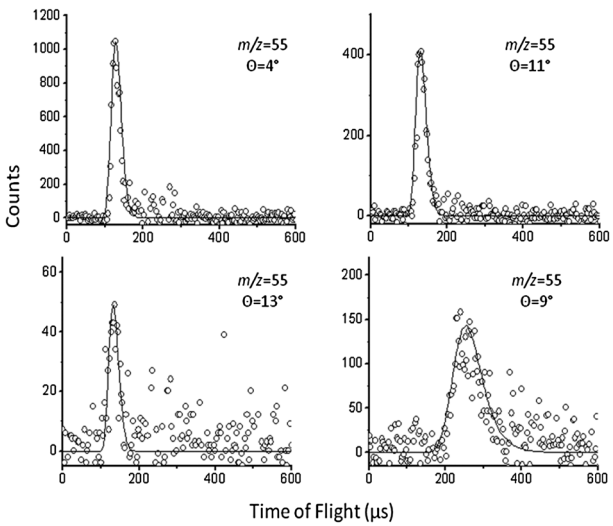

Fig. 3 TOF spectra for m/z = 55 ($C_4H_7^+$) fragments collected at Θ_{lab} = 4°, 11° and 13° using He as a seeding gas and 9° using Ne obtained from 193 nm photodissociation of C_4H_8. The fits to these TOF spectra are generated from the P(E_T) distribution in Fig. 6.

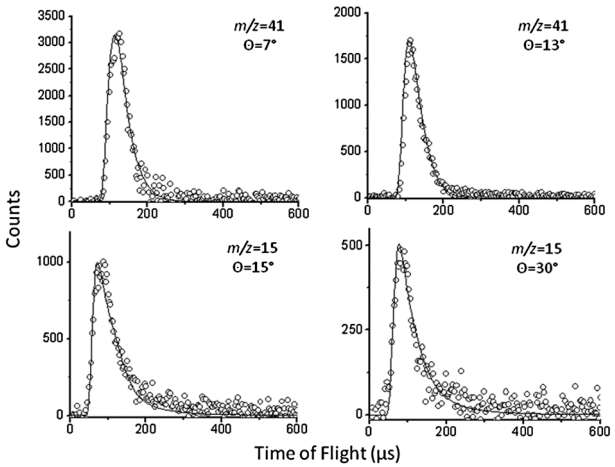

Fig. 4 TOF spectra for m/z = 41 ($C_3H_5^+$) and m/z = 15 (CH_3^+) fragments collected at Θ_{lab} = 7°, 13° and Θ_{lab} = 15°, 30° respectively obtained from 193 nm photodissociation of isobutene(C_4H_8). A single P(E_T) distribution, shown in Fig. 7, was used to fit these spectra.

Many more TOF spectra were taken at various ion masses and angles. For example, Fig. 5 shows several TOF spectra taken at m/z = 39 ($C_3H_3^+$) using Ne as the carrier gas; these spectra are particularly useful for determining the product branching ratio as discussed in Section IV.

The TOF spectra for m/z = 55 (Fig. 3, He and Ne carrier gas) consist of a single peak whose intensity decreases with increasing laboratory angle from 4° to 13°. No signal was observed beyond 13°, the kinematic limit for H atom loss at 193 nm based on the appropriate Newton diagram. Hence, since we are only observing a single peak for m/z = 55 that disappears beyond 13°, we can attribute this feature to H atom loss from the isobutene molecule at 193 nm. While the m/z = 41 and 15 spectra in Fig. 4 could, in principle, originate from dissociative ionization of the C_4H_7 fragment, these spectra extend over a much larger angular range, indicating they correspond to at least one additional photodissociation channel, with channel 2 as the likely candidate. The definitive assignment of these features is presented in Section IV.

IV. Analysis

The data were analyzed by constructing photofragment center-of-mass translational energy and angular distributions P(E_T, θ) for all photodissociation channels and using these to simulate the laboratory-frame TOF spectra. For each channel, the overall distribution can be decoupled into a product of center-of-mass translational energy P(E_T) and angular distributions I(θ) as follows:

$$P(E_T, \theta) = P(E_T)I(\theta) \quad (3)$$

The TOF spectra were fit by forward convolution of center-of-mass energy and angular distributions using the PHOTRAN software package.[26] In our experimental geometry, an anisotropic angular distribution in the plane of detection can occur even with an unpolarized laser beam since the rotational axis of the detector is orthogonal to the plane defined by the molecular and the laser beam, but a satisfactory fit to all the data was obtained assuming an isotropic distribution. The entire set of TOF data could be fit using the P(E_T) distributions in Fig. 6 and 7 for channels 1 and 2, respectively; the simulated spectra obtained from these distributions are shown as solid lines in Fig. 3, 4, and 5.

From conservation of energy, the translational energy E_T, is given by:

$$E_T = h\nu + E_0 - E_{int} - D_0 \quad (4)$$

Here $h\nu$ is the photon energy at 193 nm, D_0 the dissociation energy of a given photodissociation channel (from eqn (1) and (2)), E_{int} is the internal energy of the photofragment and E_0 is the initial energy of the isobutene molecule. Hence, for a given photodissociation channel of cold molecules (*i.e.*, E_0 = 0), the maximum translational energy E_{Tmax} is given by $h\nu - D_0$, yielding values of 60 and 47 kcal mol^{-1} for channels 1 and 2, respectively, based on the energetics of Fig. 1. This constraint was applied to the P(E_T) distributions used to fit the data; other than that, the point-wise distributions were adjusted freely to obtain the best simulation of the full data set.

The P(E_T) distribution for channel 1 in Fig. 6 fits the entire set of TOF spectra at m/z = 55. The distribution peaks at 4 kcal mol^{-1} with an average translational energy, $\langle E_T \rangle$ = 11.1 kcal mol^{-1}, and extends up to E_{Tmax} = 60 kcal mol^{-1}. The simulations are not particularly sensitive to products with

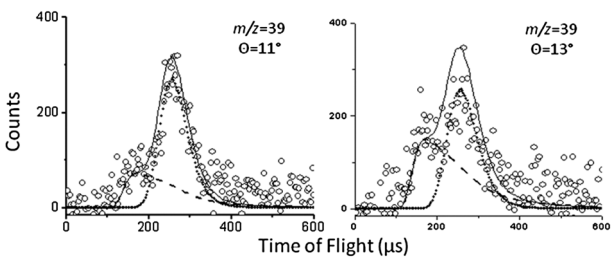

Fig. 5 Representative TOF spectra of m/z = 39 ($C_3H_3^+$) at laboratory angles of Θ_{lab} = 11° and 13°. The doted and dashed lines show simulated TOF spectra using the P(E_T) distributions in Fig. 6 and 7 respectively. The solid line shows the sum of dashed and dotted simulations.

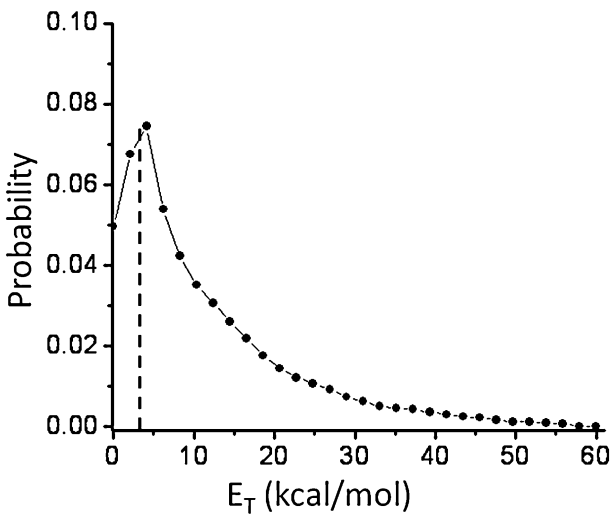

Fig. 6 Center-of-mass P(E_T) distribution from isobutene photodissociation at 193 nm to H + C_4H_7. The maximum available translational energy is 60 kcal mol^{-1}. Products with E_T < 4.5 kcal mol^{-1} can undergo secondary dissociation (see text).

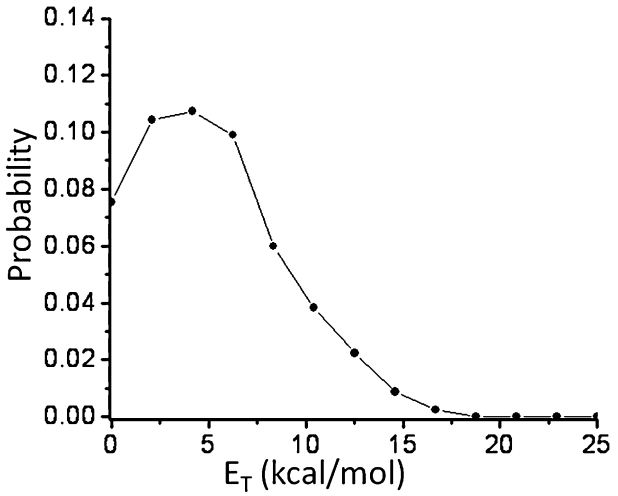

Fig. 7 Center-of-mass P(E_T) distribution from isobutene photodissociation at 193 nm to CH_3 + C_3H_5. The maximum allowed translational energy is 47 kcal mol^{-1}.

E_T < 4 kcal mol^{-1}, a point covered further in Section V, but the tail extending out to E_{Tmax} produces a better fit to our data than distributions with a lower energy cutoff.

Forward convolution of the P(E_T) distribution in Fig. 7 shows that the TOF spectra for m/z = 41 and m/z = 15 in Fig. 4 correspond to momentum-matched C_3H_5 and CH_3 photofragments from mass channel 2. The P(E_T) distribution for this channel peaks at 4 kcal mol^{-1} with an average translational energy of 5.1 kcal mol^{-1} and extends to up to 17 kcal mol^{-1}. The P(E_T) distribution could be extended to E_{Tmax} (47 kcal mol^{-1}) without degrading the quality of the fit. The analysis shows that contributions to the TOF spectra in Fig. 4 from dissociative ionization (from m/z = 41 and 55) are negligible. Fig. 1 shows that that the primary product of the photodissociation of isobutene *via* a methyl loss can further isomerize *via* a 1,2-hydrogen shift to form the allyl radical,[22] a process considered further in Section V.

The channel 2 : channel 1 branching ratio can be extracted from TOF spectra at ion masses where both channels contribute *via* dissociative ionization, such as the m/z = 39 spectra shown in Fig. 5. The branching ratio is obtained from eqn (5).

$$\frac{\text{CH}_3 \text{ loss channel}}{\text{H loss channel}} = R \times \frac{\sigma_{C_4H_7}}{\sigma_{C_3H_5}} \times \frac{f_{C_4H_7}}{f_{C_3H_5}} \qquad (5)$$

Here, R describes the relative weight of the two P(E_T) distributions used to fit the experimental data for both channels in order to reproduce the relative intensity of each contribution of the H loss and CH_3 loss channel. The relative electron impact ionization cross section, σ_i, has been determined using the additivity method proposed by Fitch *et al.*[27] Finally, f represents the fraction of a given photodissociation channel signal appearing at m/z = 39 *via* dissociative ionization. These fractions, 30% for the H loss channel and 49% for CH_3 loss, were determined by taking TOF spectra at Θ_{lab} = 9° at all values of m/z that yield to a measurable signal (m/z = 55, 54, 53, 52, 51, 50, 49, 41, 40, 39, 38, 37, 36, 27, 26 and 25). Fig. 5 shows two representative TOF spectra for m/z = 39 and indicates the simulated contributions of dissociative ionization from channels 1 and 2; the simulations are generated from the P(E_T) distributions in Fig. 6 and 7. By optimizing R to generate the best agreement with the TOF spectra, we obtained a branching ratio of 1.7 (5) in favor of CH_3 loss. The main source of uncertainty for the branching ratio comes from the determination of R which may vary between 1.5 and 2.5 with best agreement found at 2.1.

Finally, electronic structure calculations were carried out to characterize the reaction coordinates for channels 1 and 2, *i.e.* C–H and C–C bond cleavage. The calculations were performed at the MP2/6-311 + g(d,p) level of theory and basis set using the GAUSSIAN03[28] software package. The reaction coordinates were mapped out optimizing the geometry as either r_{CH} or r_{CC} was varied. Calculations were carried out to bond lengths as large as 3.8 Å for both bonds. The optimized bond lengths were found to be r_{CH} = 1.093 Å and r_{CC} = 1.506 Å at the equilibrium geometry. No exit barrier was found for either channel, as expected for simple bond cleavage. Calculated energies along the two reaction coordinates were scaled to match ΔH_0 of eqn (1) and (2); these scaled energies were used in the RRKM calculations described in Section V. Harmonic vibrational frequencies were calculated for vibrational modes perpendicular to both reaction coordinates for use in RRKM rate constant calculations discussed in Section V.

V. Discussion

The preceding analysis shows that photodissociation of isobutene at 193 nm results in both H and CH_3 loss as primary photofragmentation channels. The P(E_T) distributions for both channels in Fig. 6 and 7 peak at low kinetic energy. This result, in conjunction with our electronic structure calculations that show no exit barrier for either channel, suggests that the overall dissociation mechanism involves internal conversion to the ground state followed by statistical unimolecular decay to products. If this is the case, however, then we need to be able to explain why the CH_3 loss channel is favored even though it lies higher in energy by ~13 kcal mol^{-1}, assuming that the other fragment is the 2-propenyl radical. In the remainder of this section, we consider various aspects of the two channels in more detail and conclude by discussing calculations of the branching ratio using RRKM theory.

The P(E_T) distribution for channel 1 shown in Fig. 6 peaks at 4 kcal mol^{-1}. However, as indicated in Fig. 1, the 2-methylallyl radical formed *via* H atom loss can undergo further dissociation to CH_3 + C_3H_4; the calculated barrier for this process is 55.5 kcal mol^{-1}.[21] Any C_4H_7 fragments from channel 1 with internal energy exceeding this barrier height can undergo secondary dissociation. Since the H atom has no internal excitation, the C_4H_7 internal energy is given by $E_{Tmax} - E_T$, so fragments with E_T < 4.5 kcal mol^{-1} would have enough internal energy to dissociate. We found that a P(E_T) distribution truncated below 4.5 kcal mol^{-1} (shown as a dotted line in Fig. 6) produced fits to our data at m/z = 55 that are indistinguishable from those generated from the distribution in Fig. 6, so we cannot claim to see clear evidence for secondary dissociation. However, if this process is occurring, it only affects a small part of the P(E_T) distribution and will not significantly alter the calculated branching ratio.

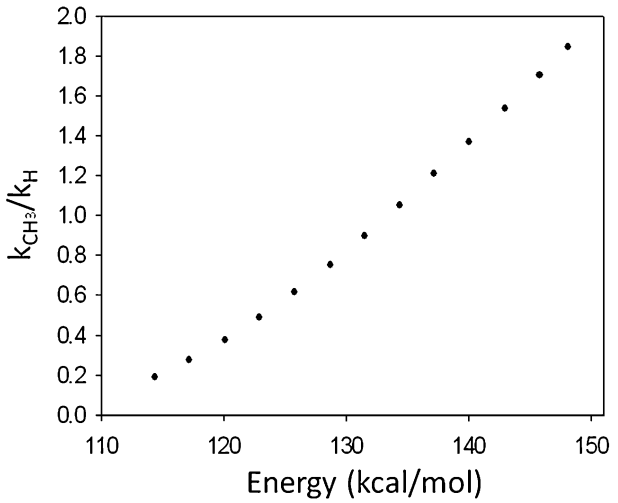

Fig. 8 Evolution of the rate constant ratio calculated using RRKM theory between the CH_3 loss channel and the H loss channel at fragment separation of 3.4 Å as a function of energy.

For channel 2, the C–C bond fission products are CH_3 + CH_3CCH_2, the 2-propenyl radical. As seen in Fig. 1, this species lies 20.6 kcal mol^{-1} above the allyl radical,[22] and one must then consider the possible role of allyl in the dissociation dynamics. For example, it is possible for allyl to be formed directly from the dissociation of isobutene through a multi-center transition state, in which an H atom from the remaining CH_3 group transfers to the central C atom as the methyl fragment departs. Such a transition state typically results in a substantial exit barrier along the reaction coordinate which would then lead to a translational energy distribution peaking well away from $E_T = 0$, in contrast to the distribution in Fig. 7. Hence concerted production of allyl seems unlikely.

It is also possible for 2-propenyl products formed with more than 45.4 kcal mol^{-1} internal energy to isomerize to allyl by a 1,2-hydrogen shift, according to the energetics in Fig. 1. However, since E_{Tmax} for channel 2 is only 47 kcal mol^{-1} at 193 nm, this means that isomerization can only occur for dissociation events with $E_T < 1.6$ kcal mol^{-1}, which corresponds to a very small fraction of the P(E_T) distribution in Fig. 7. Moreover, this value of E_T assumes no internal excitation of the CH_3 fragment. Isomerization to allyl therefore represents a very minor contribution to the overall dynamics and may not occur at all.

It thus appears that our channel 2 : channel 1 branching ratio of 1.7 (5) favors the higher energy C–C bond fission channel over C–H bond fission, a somewhat unexpected result at first glance. However, as discussed in previous work on isobutene kinetics,[13,14] the A-factor for CH_3 loss is higher than for H loss because CH_3 loss results in three more rotational degrees of freedom at the transition state than H loss. As a result, CH_3 loss should become faster than H loss at a sufficiently high temperature.

We have explored this effect from the perspective of our experiment by calculating microcanonical rate constants $k_i(E)$ for the two channels with RRKM theory,[29]

$$k_i(E)\frac{W^*(E-E_0)}{h\rho(E)} \quad (6)$$

Here W^* defines the total number of states of the critical configuration, E_0 is the energy of the transition state, and $\rho(E)$ denotes the density of states of the reactant at total energy E. The density and sum of states were calculated by direct state-count method using the Beyer-Swinehart algorithm,[30,31] using vibrational frequencies obtained from the electronic structure calculations described in Section IV. Vibrational frequencies for all modes perpendicular to the reaction coordinate were calculated for both bond fission channels. For $r_{CC} > 2.6$ Å, we treated torsional motion of the methyl group as a one-dimensional free rotor with a rotational constant of around 5 cm^{-1}.

By looking at the evolution of the calculated rate constants for both channels as a function of fragment separation, we found minimum values of the rate constants for channels 1 and 2 at $r_{CH} = 3.4$ Å and $r_{CC} = 3.4$ Å, respectively. These values were $k_{CH_3} = 1.55 \times 10^8$ s^{-1} and $k_H = 8.42 \times 10^7$ s^{-1}, leading to a theoretical branching ratio of CH_3 loss : H loss of 1.8, in remarkably close agreement with experiment. We also calculated the branching ratio as a function of excitation energy at these two transition state geometries as shown in Fig. 8. At 193 nm excitation (148 kcal mol^{-1}), methyl loss dominates over H loss. However, the H loss channel becomes more important with decreasing photon energy (*i.e.* increasing wavelength) to become the dominant channel at about 133 kcal mol^{-1} (215 nm), which is below the 205 nm onset[15] of the isobutene UV absorption spectrum. In any case, our RRKM results are certainly consistent with the arguments put forth in kinetics papers regarding the A-factors for the two bond fission channels and suggest that both channels should be considered when constructing kinetic models for isobutene pyrolysis and oxidation.

VI. Conclusions

We have investigated the photodissociation dynamics of the isobutene molecule at 193 nm using photofragment translational spectroscopy. The translational energy distribution and the product branching ratio between H and CH_3 loss were obtained. The translational energy distributions indicated that both channels take place *via* statistical dissociation on the ground state potential energy surface. The branching ratio between both channels was determined experimentally to be 1.7(5) in favor of the higher energy CH_3 loss channel. Electronic structure calculations combined with RRKM theory showed that such a result is consistent with statistical dissociation at the excitation energy used in our experiment.

Acknowledgements

This work was supported by the Director, Office of Basic Energy Sciences, Chemical Sciences Division of the U.S. Department of Energy under Contract No. DE-AC02-05CH11231.

References

1 V. Dias and J. Vandooren, *Fuel*, 2010, **89**, 2633.
2 S. Sato and R. J. Cvetanovic, *Can. J. Chem.*, 1958, **36**, 970.
3 T. Berndt and O. Boge, *J. Atmos. Chem.*, 1995, **21**, 275.
4 D. E. Woon and J. Y. Park, *Icarus*, 2009, **202**, 642.

5 M. J. Nam, S. E. Youn and J. H. Choi, *J. Chem. Phys.*, 2006, **124**, 8.
6 M. Zierhut, W. Roth and I. Fischer, *J. Phys. Chem. A*, 2004, **108**, 8125.
7 B. Negru, G. M. P. Just, D. Park and D. M. Neumark, *Phys. Chem. Chem. Phys.*, 2011, **13**, 8180.
8 J. N. Bradley and K. O. West, *J. Chem. Soc., Faraday Trans. 1*, 1976, **72**, 558.
9 K. Brezinsky and F. L. Dryer, *Combust. Sci. Technol.*, 1986, **45**, 225.
10 H. J. Curran, M. P. Dunphy, J. M. Simmie, C. K. Westbrook and W. J. Pitz, *Symp. (Int.) Combust., [Proc.]*, 1992, **24**, 769.
11 J. C. Bauge, F. Battin-Leclerc and F. Baronnet, *Int. J. Chem. Kinet.*, 1998, **30**, 629.
12 S. Santhanam, J. H. Kiefer, R. S. Tranter and N. K. Srinivasan, *Int. J. Chem. Kinet.*, 2003, **35**, 381.
13 K. Yasunaga, Y. Kuraguchi, R. Ikeuchi, H. Masaoka, O. Takahashi, T. Koike and Y. Hidaka, *Proc. Combust. Inst.*, 2009, **32**, 453.
14 A. Fahr, J. B. Halpern and D. C. Tardy, *J. Phys. Chem. A*, 2007, **111**, 6600.
15 E. P. Carr and H. Stucklen, *J. Chem. Phys.*, 1936, **4**, 760.
16 M. Caricato, G. W. Trucks, M. J. Frisch and K. B. Wiberg, *J. Chem. Theory Comput.*, 2010, **6**, 370.
17 M. H. Palmer, A. J. Beveridge, I. C. Walker and T. M. Abuain, *Chem. Phys.*, 1987, **117**, 51.
18 K. B. Wiberg, A. E. de Oliveira and G. Trucks, *J. Phys. Chem. A*, 2002, **106**, 4192.
19 P. G. Wenthold, M. L. Polak and W. C. Lineberger, *J. Phys. Chem.*, 1996, **100**, 6920.
20 J. L. Miller, *J. Phys. Chem. A*, 2004, **108**, 2268.
21 Y. Li, H. L. Liu, Z. J. Zhou, X. R. Huang and C. C. Sun, *J. Phys. Chem. A*, 2010, **114**, 9496.
22 H. J. Deyerl, I. Fischer and P. Chen, *J. Chem. Phys.*, 1999, **110**, 1450.
23 Y. T. Lee, J. D. McDonald, P. R. Lebreton and D. R. Herschbach, *Rev. Sci. Instrum.*, 1969, **40**, 1402.
24 J. C. Robinson, S. A. Harris, W. Sun, N. E. Sveum and D. M. Neumark, *J. Am. Chem. Soc.*, 2002, **124**, 10211.
25 S. J. Goncher, D. T. Moore, N. E. Sveum and D. M. Neumark, *J. Chem. Phys.*, 2008, **128**, 114303.
26 S. A. Harich, *PHOTRAN*, 2003.
27 W. L. Fitch and A. D. Sauter, *Anal. Chem.*, 1983, **55**, 832.
28 M. J. Frisch, G. W. Trucks, H. B. Schlegel, G. E. Scuseria, M. A. Robb, J. R. Cheeseman, G. Scalmani, V. Barone, B. Mennucci, G. A. Petersson, H. Nakatsuji, M. Caricato, X. Li, H. P. Hratchian, A. F. Izmaylov, J. Bloino, G. Zheng, J. L. Sonnenberg, M. Hada, M. Ehara, K. Toyota, R. Fukuda, J. Hasegawa, M. Ishida, T. Nakajima, Y. Honda, O. Kitao, H. Nakai, T. Vreven, J. A. Montgomery, Jr., J. E. Peralta, F. Ogliaro, M. Bearpark, J. J. Heyd, E. Brothers, K. N. Kudin, V. N. Staroverov, R. Kobayashi, J. Normand, K. Raghavachari, A. Rendell, J. C. Burant, S. S. Iyengar, J. Tomasi, M. Cossi, N. Rega, J. M. Millam, M. Klene, J. E. Knox, J. B. Cross, V. Bakken, C. Adamo, J. Jaramillo, R. Gomperts, R. E. Stratmann, O. Yazyev, A. J. Austin, R. Cammi, C. Pomelli, J. W. Ochterski, R. L. Martin, K. Morokuma, V. G. Zakrzewski, G. A. Voth, P. Salvador, J. J. Dannenberg, S. Dapprich, A. D. Daniels, Ö. Farkas, J. B. Foresman, J. V. Ortiz, J. Cioslowski and D. J. Fox, *R. A. Gaussian 09*, Gaussian, Inc., Wallingford, CT, 2009.
29 R. A. Marcus and O. K. Rice, *J. Phys. Chem.*, 1951, **55**, 894.
30 T. Beyer and D. F. Swinehart, *Commun. ACM*, 1973, **16**, 379.
31 R. G. Gilbert and S. C. Smith, *Theory of unimolecular and recombination reactions*, Blackwell Scientific Publications Journal, Oxford, 1990.

